

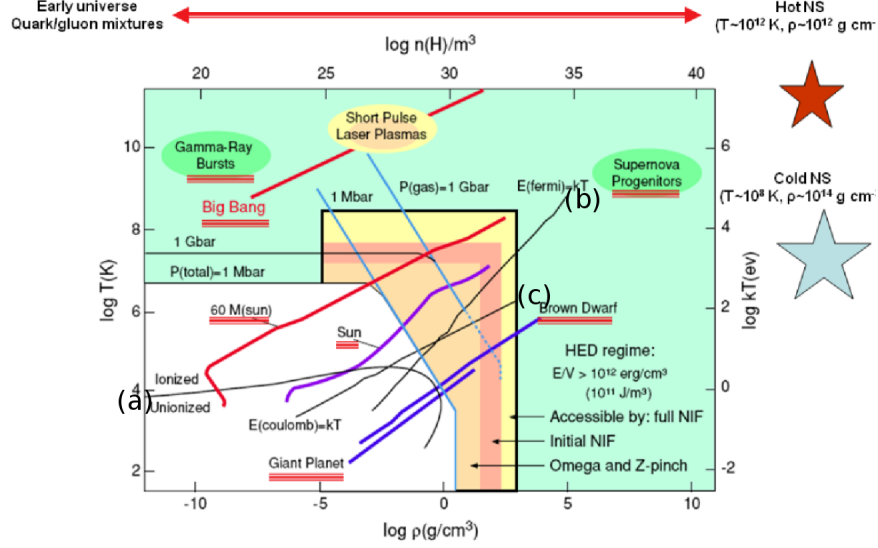
Chapter 1

INTRODUCTION

In this thesis I introduce the development of new techniques for the production of materials in the warm dense matter (WDM) regime, and for interrogation of the structure and thermodynamic state of such systems using x-ray diffraction and (to a lesser extent) spectroscopy. The main developments include a scheme for single-shot determination of the static structure factors of WDM systems generated at laser plasma facilities; a new technique for enhancing the density of deposited energy in WDM generated at fourth-generation X-ray sources such as the Linac Coherent Light Source (LCLS); and experimental results from an LCLS experiment that puts new constraints on the thermalization (both electronic and lattice) of a solid state material upon fs-scale XFEL heating. In addition to this WDM-focused research I discuss some secondary work on the development of software and electronics for energy- and position-sensitive pixel detectors including current applications in the context of soft x-ray laboratory and possible future ones in XFEL, synchrotron, and laser plasma facility-based experiments.

Before proceeding it is useful to define WDM in terms of the microphysical context it occupies. Fig. (which figure) presents a map of thermodynamic parameter space, with the logarithm of density and temperature on the horizontal and vertical axes, respectively. A few bounding curves can be identified. First, ionization occurs at temperatures exceeding approximately 1 eV; this is denoted by curve (a), which forms a boundary between the plasma and condensed matter regimes. Second, curve (b) indicates the boundary at which the Fermi energy is approximately equal to the average thermal energy $k_B T$; i.e. where the electron degeneracy parameter, $E_f/k_B T$ is of order unity. Third, curve (c) corresponds to a value of 1 for the ratio of the Coulomb energy to the thermal one, also called

Figure 1.1: The atlas of high-energy density physics (cite)



the plasma coupling parameter Γ .

Above curves (a), (b) and (c) is the regime of classical plasma physics where, as a result of the weak interaction between neighboring ions ($\Gamma \ll 1$), collective interactions predominate over binary collisions and quantum statistics can be neglected ($\Lambda \ll 1$) except for the purpose of calculating blackbody spectra. In this regime continuous, classical modeling treatments are widely-used and fully validated (cites). Below curves (a), (b), and (c) is the low-temperature, intermediate-density realm of condensed matter physics, where the established theoretical framework is that of many-body quantum mechanics, wherein the potential landscape is built on the interaction between electrons and ion cores. In this framework finite-temperature effects are incorporated perturbatively. WDM occupies the transitional regime above curve (a) and near the intersection of curves (b) and (c), characterized by partial degeneracy and strong ion-ion coupling (Γ and Λ of order unity). As a result, treatments of plasma physics originating in the classical regime are not applicable to WDM. Solid state physics models similarly fail in the WDM regime due to large, non-perturbative effects of

finite temperature on the structure and thermodynamics of WDM (cites).

Modeling of the ionization potential depression (IPD) in a plasma is a case in point of the difficulties that manifest themselves with theoretical treatments of WDM. Adequate descriptions of IPD are given the Debye-Hueckel approximation and ion sphere model, which cover opposite regimes of high temperature and low density, and low density and high temperature, respectively. We here briefly introduce both model, with focus on the assumptions and approximations that they adopt.

The Debye-Hueckel model applies to a weakly-coupled plasma in local thermal equilibrium. It identifies the electrostatic potential in the Poisson equation with the mean field generated by a population of Maxwell-Boltzmann-distributed ions or electrolytes. This results in the Poisson-Boltzmann equation which, when solved, gives the electrostatic potential produced by an arbitrary charge distribution. The condition for validity of the Debye-Hueckel model is for the Thomas-Fermi screening length (also called the Debye length) to be much larger than the mean inter-ion separation. This condition is satisfied at comparable temperatures, but lower densities, than those encompassed by the WDM regime. (check that this is right, and cite)

In the opposite limit, the ion-sphere model describes IPD in a high-density material with $\Gamma > 1$ (in the low-temperature context IPD is more commonly referred to as pressure ionization). The picture offered by the ion-sphere model is that of a plasma with highly-correlated ion positions and therefore no close encounters between ion pairs. Each ion is treated as a sphere whose potential is unaffected by the presence of neighboring ions. (cite Stewart-Pyatt). The sphere radius is $R_0 = (3/4\pi N_i)^{1/3}$, where N_i is ion number density, while the orbital radius of the ion sphere's n th principal energy level is approximately $r_n = (n^2/Z_n)(0.529\text{\AA})$. For the n th bound state to exist it is necessary that $r_n \leq R_0$; thus, IPD manifests itself as a reduction in the number of bound states as a function of the inter-ion distance R_0 . It should be noted that, although the ion-sphere model is a frequently-used heuristic in high-temperature plasmas with near-ambient densities, it is known to be incorrect in the high-density, moderate-temperature ($\Gamma \gg 1$) regime. Neaton et al. have done ab-

initio (DFT) simulation of Li—a free electron-like material under ambient conditions—showing that, contrary to intuitive expectations and the ion-sphere model, it becomes less free-electron like at high densities and additionally loses its common bcc crystal structure. (cite Neaton 1999) Due to overlap of core electrons, the treatment of electronic wavefunctions in this regime is necessarily strongly nonperturbative—again in conflict with the ion-sphere model’s assumptions.

Leaving aside, momentarily, the ion sphere model’s limitations, we might contemplate constructing a model of ionization potential depression that reduces to the ion sphere and Debye-Hueckel models in their respective limits. Doing so is challenging because it allows none of the simplifying approximations invoked by the two limiting cases. One manifestation of uncertainty of the correct approach is the existence of two mutually-contradictory models for IPD in WDM, those of Stewart and Pyatt (cite) and Ecker and Kroll (cite). Though the Stewart-Pyatt model is more widely used and has the virtue of reproducing the ion-sphere and Debye-Hueckel behaviors (cite Crowley review article), its validity has been called into question by recent direct XFEL-measurements of IPD in Al heated to 180 eV (cite Ciricosta paper). Such conflicts exemplify the persistent difficulty of constructing models with validity accross different sub-regimes of WDM.

1.1 Motivations for study of WDM

In addition to the basic physics questions intrinsic to the WDM regime, there are a number of points of contact between WDM and particular problems in other fields. This interaction has been bolstered in recent years by rapid development of laser plasma facilities and x-ray free electron lasers (XFELs) with unprecedented experimental capability for producing WDM and probing its physical properties. This has brought many previously-intractable physical regimes into the scope of both empirical investigation and numerical simulation.

1.1.1 *Astrophysical modeling*

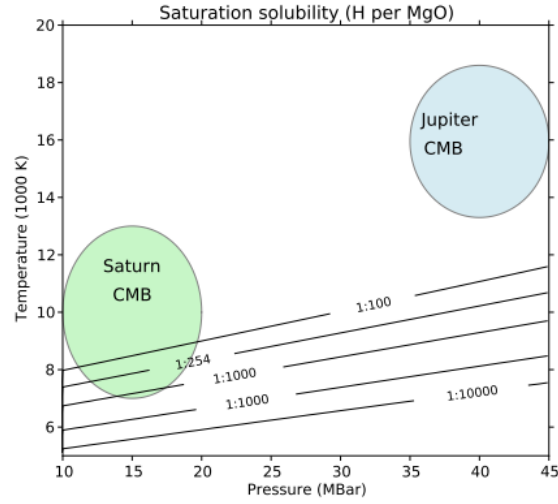
A large contribution to this growth in interest is the relevance of WDM theory as a micro-physical basis on for models of various systems in planetary and stellar astrophysics. Here we introduce two examples in which this relationship is salient.

The interiors of both rocky and gas giant planets contain dense, and in some cases Fermi-degenerate, plasmas at 1 eV-scale temperatures. Examples include the iron under conditions of the earth’s core (pressure = 3 Mbar; $T = 6000$ K), whose viscosity and equation of state (EOS) has consequences on convective heat transfer and the formation of earth’s magnetic field. (cites) Similarly, modeling of the evolution and structure of gas giant planets depends on the EOS of H under the regime of gas giant interiors. The existence of metallic H caused by pressure ionization at Mbar-scale pressures has been experimentally demonstrated, but its onset is poorly understood at the level of theoretical models for the EOS: although a first-order dielectric-to-metal phase transition has been postulated, current approaches do not attempt to model pressure ionization, instead limiting themselves to interpolation between the better-understood atomic and fully ionized limits. (cites)

The solubility physics of two-component WDM mixtures containing H with other species found in rocky planetary bodies has direct consequences on mass transport accross the core-mantle boundary in gas giant planets. It also has crucial importance in the modeling of gas giant formation, where the solubility of H with rocky elements bears on the plausibility of the planetesimal accretion hypothesis for gas gian genesis, which requires condensation of H and He around a rocky core. (cite Wilson MgO solubility paper).

Another case in which the material properties of warm dense matter determine the behavior of an astrophysical object is that of white dwarves, whose envelopes consist of a hot, partially Fermi-degenerate plasma. Modeling the cooling of white dwarves is a topic of interest (cites), especially in the context of the importance of type 1a supernovae as ‘standard candles’ for measuring distances to distant galaxies. Doing so, however, requires knowledge of stellar envelope opacities, equations of state (EOS), and transport properties, many of which

Figure 1.2: Saturation solubility of MgO in H as a function of pressure and temperature from *ab initio* calculation by Wilson et al. The temperature conditions of the core-mantle boundaries of Saturn and Jupiter are indicated. (cite Wilson)



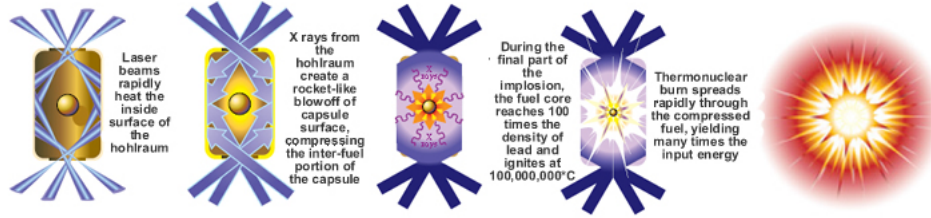
properties are currently unknown to within factors of order unity. The absence of understanding of the simplest available system—the hydrogenic one-component plasma—underscores the difficulty of this thread of research.

1.1.2 Inertial Confinement Fusion

The effort to reach controlled fusion through implosion of deuterium-tritium fuel capsules—an approach termed inertial confinement fusion—has progressed significantly in the last decade due to completion of laboratory facilities capable of producing HED (definition?) plasmas with densities and temperatures approaching levels needed for ignition. Fig. (which figure) shows a schematic of an ignition technique called indirect drive. In this configuration the ICF target, which consists of a hollow spherical capsule of ablator material filled with deuterium-tritium fuel, is confined in a hollow capsule of a high-Z material (the Hohlraum). A multi-TW, ns-duration laser passes through apertures in the Hohlraum and heats the Hohlraum to blackbody temperatures on the order of several hundred eV. The resulting thermal spectrum of soft X rays isotropically heats and ablates the fuel capsule's surface,

causing its interior to implode by conservation of momentum. Typical parameters of the plasma created at maximum compression include areal densities (capsule density \times radius) of 0.3 g/cm^2 and temperatures of the order 10 keV . (cite. see x-games pg 113)

Figure 1.3: Schematic of indirect-drive inertial confinement fusion shot. (cite)



Although its end state falls well within the regime of a classical plasma, the fuel capsule transitions through the WDM state during compression. The opacity and EOS of warm dense matter therefore has a strong influence on the development and propagation of shocks during ablation of the fuel capsule, which in turn affects the optimization of various experimental parameters, including fuel capsule geometry and temporal profile of the laser driver. Accurate modeling of the fuel capsule's transport properties under the WDM regime is equally important for understanding the development during compression of hydrodynamic instabilities, which are known to be a major obstacle to the efficient coupling of laser energy into fuel compression (cites).

1.2 Experimental Generation of WDM

WDM conditions may be generated using X-ray free electron lasers (XFELs) and several varieties of lasers, found both in large-scale facilities and laboratory-scale systems. Here we provide an overview of existing technologies.

1.2.1 Long-pulse lasers

Lasers with pulse durations on the order of nanoseconds and energies of 1 kJ or more are among the most versatile tools for producing high energy density states, including warm

dense matter. In the most common use cases of long pulse lasers the target is a bulk material, and coupling of laser energy into it occurs in two stages. First, the laser rapidly (TODO how rapidly) generates a coronal plasma at the material’s surface. Once the electron density of this plasma exceeds the laser wavelength’s critical density (TODO: equation) the laser becomes electromagnetically shielded from the material’s interior and can no longer transfer energy to it. In the context of direct drive (where the material is a target to which laser energy is directly coupled), subsequent energy transfer occurs by thermal conduction of energy from the surface plasma to higher-density regions as well as by compression of the target resulting from ablation of its surface. In the case of indirect drive, the laser’s energy is used to heat a surface (typically the interior of a Hohlraum) that provides a thermal bath which, in turn, couples to the target via its blackbody radiation.

The ns duration of long-pulse lasers matches the timescale on which mechanical and hydrodynamic processes occur on typical target scales. Long-pulse lasers are thus suited to generating ramp and shock compression, notably including for the application of ICF. The largest-scale laser plasma facilities—Omega EP at the Laboratory for Laser Energetics in Rochester, NY and the National Ignition Facility—are long-pulse laser systems targeted toward the ICF program.

1.2.2 Short-pulse lasers

Short pulse lasers are a second class of systems used to generate HED conditions. They are typically defined by pulse durations on the order of a picosecond or less, down to as little as ~ 1 fs.

Short-pulse laser systems arose after the development of chirped pulse amplification in the 1980s (cite) and have proliferated ever since (cites), especially with the recent advent of compact (university laboratory-scale) versions with tens of Joules of pulse energy, sufficient to generate scientifically interesting HED conditions. The largest-scale short pulse lasers have pulse powers up to 100 TW (check this number), with durations between 10 and 100 fs (check this as well).

Due to the smaller total energies of short-pulse lasers and the relatively slow cooling timescale of materials heated above ambient conditions *regardless* of the pump duration, short-pulse lasers are used to generate HED conditions under direct-drive configurations alone. Energy is coupled into a target indirectly (as is the case with long-pulse systems) via ‘hot’ MeV-scale electrons generated in the laser’s interaction with plasma at the target surface. In the (typical) case where bulk heating is required, the target thickness is small compared to the hot electrons’ stopping range, causing them to reflux through the target once it acquires net positive charge. This process lasts on the order of one ps (check this, cite Nilson and maybe others) and thus sets the time resolution of experiments in which the short-pulse laser is used to both heat and probe the target.

1.2.3 X-Ray Free Electron Lasers

The advent of X-Ray Free Electron lasers is a major advance in capability for WDM research. Existing incarnations of these sources, notably the Linac Coherent Light Source (LCLS), provide 10^{14} photons in a ≥ 10 fs-duration monochromatic pulses with tunable energy. While the energies per pulse are smaller than those attainable with a short-pulse laser, they are largely sufficient to produce HED states with temperatures in excess of 100 eV (cite). Because XFELs can heat volumetrically, they are free of the primary deficiency of lasers with respect to the task of generating dense plasmas: namely, the latter can only heat bulk materials indirectly and over durations of 1 ps or longer, which exceeds the timescale for changes in WDM, preventing the study of short-lived transient states.

The ability to generate (and probe) WDM on truly inertial timescales, wherein atomic nuclei are effectively frozen, has been duly exploited in early pioneering studies at the LCLS. It forms the basis, for example, for a new thread of materials science research on nonthermal lattice and spin dynamics (cite Lee and others). Likely even more significantly, it is the enabling feature for macromolecular crystallography under the ‘diffract before destroy’ paradigm. (cites) The possibilities surrounding rapid generation of WDM is a topic to which I return in (which chapter?). (cite Vinko et al. and other early LCLS papers).

1.3 X-ray diagnostics of WDM

Experimental studies of WDM suffer from a substantial complication: the opacity of WDM to photons is large at energies up to the soft X ray regime. As mentioned in section 1.2.2, in the context of laser heating this is merely a frustration; for the purposes of measuring the conditions of a bulk WDM system, however, the need for direct detection of radiation originating from the target's interior makes optical probes wholly ineffective. Determination of the structure and thermodynamic state variables of a dense plasma therefore requires sufficiently penetrating radiation; for this reason, the large majority of WDM diagnostics are X ray photon-in photon-out measurements.

In the remainder of this section I provide an overview of the various available X-ray techniques.

1.3.1 Scattering

Elastic scattering and nonresonant inelastic X-ray scattering (NIXS) are among the most-frequently probed signals for inferring the structure, temperature and ionization state of WDM. In dense plasmas generated by long-pulse lasers, where LTE is commonly assumed, NIXS also serves as a probe of temperature.

For a given sample, the sum of scattering interactions is characterized by the double-differential scattering cross section (DDCS) $d^2\sigma/d\Omega d\omega$, which describes the probability of a photon to scatter into a solid angle increment $d\Omega$ within an energy loss interval $d\omega$. Within the independent-electron and first Born approximations the DDCS is given by

$$\frac{d^2\sigma}{d\Omega d\omega} = r_0^2 \left(\frac{\omega_2}{\omega_1}\right) |\epsilon_1 \times \epsilon_2^*|^2 S(\vec{q}, \omega), \quad (1.1)$$

where

$$S(\vec{q}, \omega) \equiv \sum_F \sum_j \langle F | \exp(i\vec{q} \cdot \vec{r}_j) | I \rangle|^2 \delta(E_F - E_I - \hbar\omega). \quad (1.2)$$

The first term in equation 1.3.1 is the Thomson cross section, which describes the interaction between a probe photon and a single electron; $S(\vec{q}, \omega)$ is referred to as the dynamic structure factor, and encapsulates all system-specific properties. I and F are initial and final states of the sample with energies E_I and E_F , respectively, and the second summation of 1.3.1 is over electrons in the scatterer.

Following Chihara (cite Chihara), the typical treatment of a dense plasma separates the dynamic structure factor into several components:

$$S(\vec{q}, \omega) = |f_I(q) + f_e(q)|^2 S_{ii}(q, \omega) + S_{ff}(q, \omega) + S_{bf}(q, \omega), \quad (1.3)$$

S_{ii} is the atomic/ionic structure factor, f_I and f_e are the form factors for the ion and a surrounding cloud of screening charge. S_{ff} contains scattering from free, delocalized electrons, and S_{bf} represents Raman-type bound-free transitions resulting from scattering from tightly-bound core level electrons. Note that spherical symmetry has been assumed: all terms of the structure factor depend only on the magnitude of \vec{q} .

The first term corresponds to elastic ($\omega = 0$) scattering, and is connected to the dense plasma's pair distribution function by a Fourier transform. Though not a component of the NIXS signal, it must often be considered in simulations and analyses of NIXS data, wherein the Bethe sum rule (cite) and other conserved quantities consist of integrals over the entire energy-loss domain of the dynamic structure factor. Elastic scattering is a highly-useful probe of structure; we consider it separately in section 1.3.1.

The free-free contribution to $S(q, \omega)$ can be expressed in terms of the free-electron dielectric function $\epsilon(q, \omega)$ via the fluctuation-dissipation theorem (cite Kubo et al.):

$$S(q, \omega) = \frac{\epsilon_0 \hbar q^2}{\pi e^2 n_e} \frac{1}{1 - e^{\hbar\omega/k_B T_e}} \text{Im} \frac{1}{\epsilon(q, \omega)}, \quad (1.4)$$

The random phase approximation (RPA) (cite Bohm and Pines) is typically used as an approximation for $\epsilon(q, \omega)$, but more recent treatments incorporate a perturbative treatment of electron-ion interactions using the Born-Mermin Approximation (cite Mermin). As shown

in Fig. (which figure?), the scattering contribution of S_{ff} consists of a pair of Plasmon peaks with opposite, equal-magnitude energy offsets from the elastic scattering peak. Electron density is inferred from the magnitude of the Plasmon peak shifts while temperature is obtained from the ratio of intensities of the two peaks, following the principle of detailed balance (cite Glenzer 2007 and Lee 2009).

Although the connection of temperature and density to the free-free component of the dielectric function is well-founded, there are two obstacles to effective interpretation of collective scattering data from WDM systems; one is theoretical and the other experimental. First, the validity of established treatments of the dielectric function has been called into question, with recent plasmon spectrum calculations based on MD-DFT simulations showing a significant change in the plasmon profile compared to that predicted by the BMA. (cite Mattern thesis and Plagemann). Second, the plasmon peak suffers from poor signal to background and has a small separation from the elastic scattering peak under typical WDM electron densities, making it difficult to resolve. As a result only a handful of experiments to date have pursued this technique.

We finally turn our attention to the last term of 1.3.1, S_{bf} , whose contribution to the inelastic DDCS is often referred to as x-ray Thomson scattering (XRTS). Obtaining state variable information from a system's bound-free scattering contribution is dependent on the underlying model of electronic structure used; as a result, various treatments exist, including the Impulse Approximation (IA) of Eisenberger and Platzman, wherein the bound-free contribution to XRTS is equivalent to Doppler-broadened Compton scattering (cite Eisenberger and Platzman); the plane wave form factor approximation (PWFFA) of Schumacher (cite Schumacher), which attempts to extend the IA by incorporating electron binding energies; and calculation of matrix elements using a real space Green's function (RSGF) formalism applied to atomic clusters, as implemented in the atomic spectroscopy code FEFF (cite Mattern).

In current practice, measurement of the bound-free component of XRTS from WDM is performed in the large- q regime, where the Compton feature is broad and can be measured

using high-efficiency (but low-resolution) HOPG-based spectrometers (need cites for this). As such, single-particle bound-free scattering is more readily measured than collective excitation features. Since an early demonstration of the technique by Glenzer et al. (cite Glenzer 2003) it has been frequently implemented at both laser plasma and XFEL facilities (cite figures showing how these experiments are set up). Despite some fruitful outcomes (how so? need examples, cites), the large statistical uncertainties in XRTS spectra—particularly at laser plasma facilities, where single-shot measurements are photon-starved—make the inference of state variables difficult, and dependent on one’s choice of electronic structure model (check that this is right. do predicitions heavily depend on the choice of model, or is it just that uncertainties are high, regardless of the choice?). Mattern et al. have demonstrated this concretely by comparing theoretical fits to XRTS data of shock-compressed Be, and argue that the lack of rigorous validation of electronic structure models for WDM models strongly undermines their validity for first-principles measurement of state variables. With this context as motivation, we revisit the topic of WDM thermometry in chapter (reference chapter).

1.3.2 *Coherent Scattering*

Coherent scattering is the zero-energy loss component of the double differential cross section. The inference of structural information from coherent scattering varies by material; two primary cases present themselves.

First, for amorphous materials, such as hot dense plasmas generated by ramp- or shock-compression and lacking long-range order, the scattering amplitude is isotropic and is characterized by the one-dimensional static structure factor, which is connected by a Fourier transform to the material’s pair correlation function. Inference of the full pair correlation function is in practice frustrated by the difficulty of inverting a limited momentum transfer range-sampling of the strucure factor, but even in the most information-limited scenarios a density can nevertheless be recovered from the strucure factor’s first correlation peak. Although coherent scattering measurements from dense plasmas have been demonstrated in

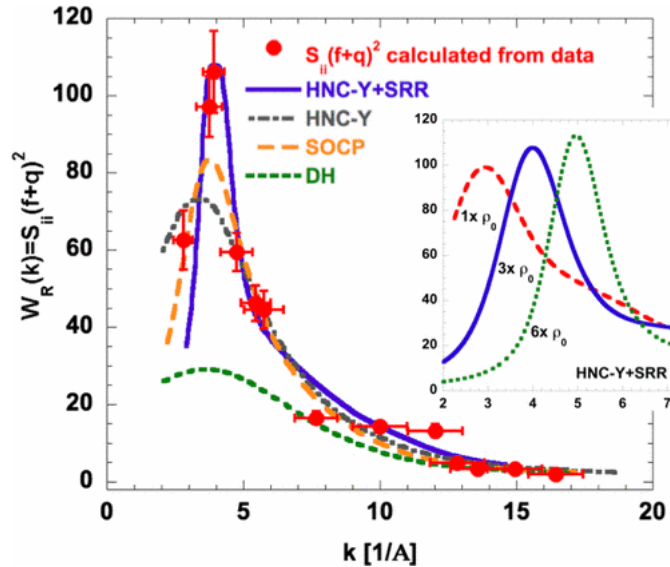
the context of long-pulse laser compression experiments, implementation difficulties unique to that environment prevent its adoption as a routine technique. We address these difficulties, and proposed solutions, in chapter (chapter reference). (cite Ma et al).

Second, in materials with long-range crystalline order, as typically found in XFEL-based experiments (whose timescales are shorter than the thermalization rate of electronic and ionic degrees of freedom), the coherent scattering amplitude is given by

$$F(\vec{q}) = \sum_n e^{i\vec{q} \cdot \vec{R}_n} \sum_j f_j(\vec{q}) e^{i\vec{q} \cdot \vec{r}_j}, \quad (1.5)$$

where the first summation is over all lattice vectors \vec{R}_n and the second, referred to as the *unit cell structure factor*, is over positions \vec{r}_j of atoms within the unit cell. By the convolution theorem, the crystal's scattering amplitude in reciprocal space is equal to the product of the lattice and unit cell structure factor. The coherent scattering signal is therefore a discrete sampling of the unit cell structure factor at individual Bragg peaks with momentum transfers corresponding to vectors of the reciprocal lattice.

Figure 1.4: Experimental elastic scattering intensity of shock-compressed Al at OMEGA-60, compared to several hypernetted chain (HNC), Debye-Hueckel (DH), and screened one-component plasma (SOCP) models. (cite Ma et al.)



In the context of XRD from a material undergoing thermalization under fs XFEL heating, the crystal scattering amplitude's decomposition into lattice and unit cell components has a direct correspondence to interpretation of structural change. The onset of long-range lattice disorder is readily identifiable as a quenching in Bragg peaks roughly proportional to e^{-q^2} . Evolution of the unit cell structure factor, on the other hand, is dependent on the details of atomic level populations and the material's finite-temperature electronic structure, and can be used as a test of competing theoretical models of both.

(need cites and discussion of the existing literature on XRD of XFEL-heated WDM)

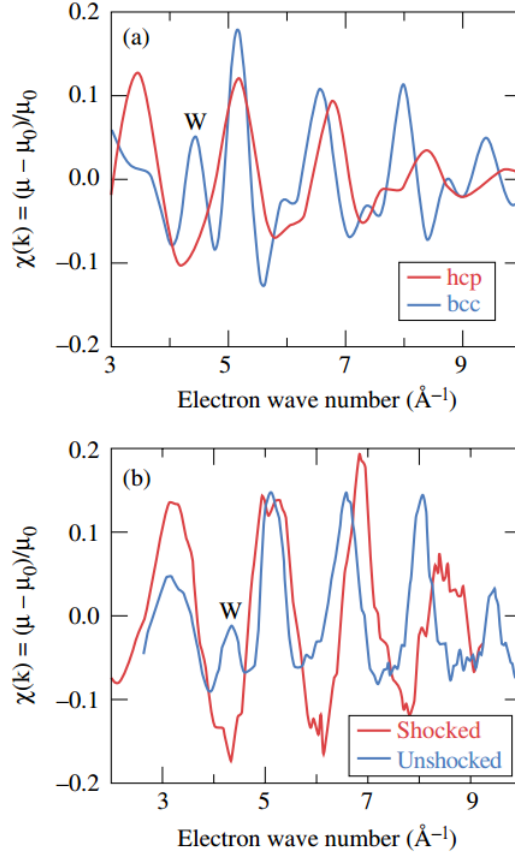
1.3.3 X-ray absorption

X-ray absorption spectroscopy (XAS) may be used to measure the structure and unoccupied electronic density of states of WDM systems. The information available by X-ray absorption near-edge spectroscopy (XANES) and X-ray absorption fine structure (XAFS) is the same as in other scientific contexts, but the experimental implementation differs in a few respects. In all instances, the short duration of WDM states requires instantaneous collection of absorption spectra using a source with broad-band spectrum. At laser plasma facilities this is arranged using a spherical capsule of CH polymer imploded using a long-pulse laser (cite yaakobi 2003) that emits a thermal spectrum with a ~ 1 MeV temperature (check this). This so-called broadband backlighter has been used to collect XAFS for the study of compression-induced phase transitions, such as that from bcc to hcp Fe driven by ns shock-compression (cite Yaakobi 2005).

XANES measurements on dense plasma have also been performed at laser plasma facilities. This requires narrower-band illumination compared with XAFS, which has been achieved using short pulse laser-driven multicomponent X-ray fluorescence backlighters. Levy et al., for example, have used this technique to demonstrate XANES-based thermometry based on measurement of the K-edge slope in Al isochorically heated to 3 eV. (cite Levy et al).

Laser wakefield accelerator X-ray sources generate fs-duration broadband X-ray emis-

Figure 1.5: FEFF calculation of XAFS for hcp and bcc phases of Fe (a), compared to experimental data taken on ambient and shock-compressed Fe at the OMEGA laser (b). (cite Yaakobi)



sion, affording time resolution that surpasses what is possible with laser-driven backlights. This makes wakefield accelerators especially well-suited to X-ray absorption spectroscopy of WDM generated at XFEL facilities (cite Albert). The combination of wakefield accelerators with XFELs promises the unprecedented possibility of XFEL pump-probe experiments with simultaneous fs-duration interrogation of the target using broad- and narrow-band hard X-rays. This combination also enables XAS measurements of low-Z materials, which is much more challenging at laser plasma facilities as a result of the mismatch between the short penetration lengths of x-rays near the K-edges of low-Z species and the relatively large target

thicknesses (tens of microns) needed for effective laser ablation.

1.3.4 X-ray Emission and X-ray Fluorescence

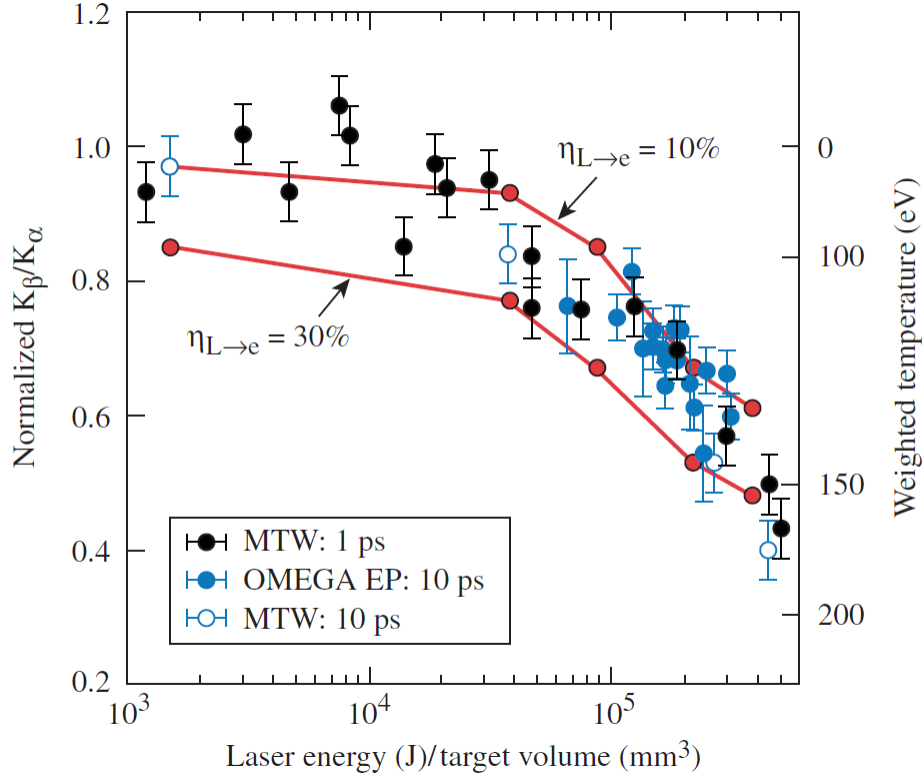
X-ray fluorescence spectroscopy (XRF) is an extensively used probe in experiments studying the interaction of high-intensity lasers with solid targets. In short-pulse laser experiments involving mid-Z elements heated to temperatures comparable to or larger than M-shell binding energies the ratio of K_β to K_α emission is used as a measurement of temperature. Modeling the coupling efficiency between high-power laser and electrons in a solid-density target is of considerable significance to the effort to understand optical radiation-matter interactions at high laser intensities ($> 10^{19}$ W/cm²); in this context, inference of target heating using K_β/K_α branching ratios provides a useful consistency check in the application of models to experimental data. (cite Myatt et al 2007, Nilson).

X-ray emission spectroscopy (XES), the finer-grained cousin of XRF, provides more detailed information on the occupied density of states in a material and can be sensitive to valence-level excitations in the ‘tepid’ transitional regime between ambient and warm dense matter states (reference XES figure from the LD67, maybe get some cites). It has seen use primarily at XFEL facilities, where higher shot rates and probe intensities make the collection of datasets with satisfactory statistical quality easier. (cite photosystem 2 XES papers). The advent of XFELs as the first high-intensity, monochromatic, and tunable WDM probes has also enabled resonant inelastic X-ray scattering (RIXS) measurements, which has made possible the direct measurement of ionization potential depression on a fs timescale, as demonstrated by Vinko et al. (cite Vinko, Ciricosta.).

1.4 Dissertation Outline

The overarching theme in this thesis is the relationship, and frequent feedback, between scientific discovery and the development of new experimental technique. To begin, in chapter 2 I introduce a scheme for single-shot measurement of the static structure factors of disordered dense plasmas produced at large-scale laser facilities such as Omega and NIF. In Chapter 3

Figure 1.6: Experimental K_α/K_β ratios of emission from Cu foil heated by short-pulse lasers, with inferred electron temperature on the right vertical axis. Model calculations are heating for hot electron coupling efficiencies η_e equal to 10% and 30% (cite Nilson)



I present an experimental observation of nonlocal heat transport by keV-scale electrons in a nanophase material and consider the question of how this effect can be used to improve WDM experiments conducted at XFELs via optimized nanostructured target design. In chapter 4 I discuss experimental results of a recent experiment at the LCLS in which we established bounds on the timescales for thermalization of the lattice in XFEL-heated metal oxides and measured the consequences of XFEL heating on electronic charge density, with subsequent comparisons to different model predictions. In chapter 5 I describe an instrument-development effort toward a disposable CMOS-based X-ray camera for use in experimental environments hostile to electronics, particularly laser plasma facilities. Finally, in chapter 6 I introduce UW-XAP, a software tool for streamlined realtime data collection and analysis

at the LCLS.